In Situ Growth of Silver Nanoparticles into Reducing-End Carbohydrate-Based Supramolecular Hydrogels for Antimicrobial Applications

Bing Chen, Elizângela Hafemann Fragal, Eric Faudry, Sami Halila

In Situ Growth of Silver Nanoparticles into Reducing-End Carbohydrate-Based Supramolecular Hydrogel for Antimicrobial Applications

Bing Chen,[a] *Elizângela Hafemann Fragal,*[a†] *Eric Faudry,*[b] *Sami Halila**[a]

[a] Univ. Grenoble Alpes, CNRS, CERMAV, 38000 Grenoble, France.

[b] CEA, INSERM, CNRS, Univ. Grenoble Alpes, UMR 1036/ERL 5261, 38054 Grenoble, France

KEYWORDS: Carbohydrate chemistry, chemoselective reactions, supramolecular hydrogels, silver nanoparticles, antibacterial.

ABSTRACT: Hydrogels with antibacterial activities have the potential for many biomedical applications, such as wound healing, because the maintaining of the moist environment and the prevent of infections. In this work, an ultrasound-induced supramolecular hydrogel consisting of easily accessible reducing-end free glucosaminylbarbiturate-based hydrogelators that serve for *in situ* fabrication of silver nanoparticles (AgNPs), excluding the addition of any external reducing or stabilizing agents, has been developed. The innovative synthetic approach relied on the use of *N,N′*-disubstituted barbituric acid derivatives as a versatile chemical platform that site-selectively reacted with amino function of glucosamine. A series of glucosaminylbarbiturate were synthesized and we identified one carbohydrate-based hydrogelator that produced a thixotropic

supramolecular hydrogel after ultrasound-mediated breaking of an intralocked hydrogen bond. AgNPs@hydrogel were prepared through *in situ* reduction of silver ions mediated by reducing properties of carbohydrates. The AgNPs@hydrogel composite revealed good antimicrobial properties towards both Gram-positive and Gram-negative bacteria. These findings contribute to the development of carbohydrate-based supramolecular hydrogels and make them promising efficient and safe soft materials for antimicrobial therapy.

1. INTRODUCTION

Over the preceding decade, the preparation of noble metal nanoparticles through environmentally conscious green synthesis methods has been extensively documented, driven by a growing awareness of environmental concerns. Among the diverse array of noble metal nanoparticles, silver nanoparticles (AgNPs) have garnered significant attention owing to their distinctive optical, electrical, catalytic, and antibacterial properties relative to bulk metallic silver. Indeed, AgNPs find widespread applications in personal care products, textiles, food packaging, construction materials, and medical instruments, owing to their remarkable and established antibacterial efficacy. Notably, Ag^+ cations have been observed to disrupt bacterial cell membranes and to inhibit the enzymatic activities of bacterial cells.[1]

In pursuit of the development of anti-infective materials tailored for biomedical applications, the incorporation of AgNPs within biocompatible matrices to facilitate a sustained release of Ag^+ cations become imperative. Hydrogels derived from natural polymers, such as polysaccharides,[2-4] have been extensively employed since they closely mimic the extracellular matrix, and the three-dimensional macromolecular network prevents the direct release of AgNPs while permitting controlled release of Ag^+ cations. Both *in situ* and *ex situ* methodologies have

been explored for the preparation of AgNPs@hydrogel composites. In the case of the *in situ* approach, Ag^+ cations initially form coordination complexes with specific chemical groups constituting the polymer hydrogels. Subsequent reduction of the Ag^+-loaded gel by a chemical reagent ensures the uniform synthesis of NPs within the gel matrix.[3, 5-7] Nonetheless, the use of a reducing agent such as $NaBH_4$ may potentially exhibit cytotoxic effects.[7-9] Therefore, to circumvent the use of toxic reducing agents, alternative chemicals such as reducing carbohydrates (glucose) or ascorbic acid, have been judiciously used.[10] In the context of the *ex situ* approach, pre-synthesized AgNPs are combined with the polymer matrix and subsequently subjected to a "cross-linking" process to induce gelation. However, the tendency of AgNPs agglomeration, attributable to their elevated active surface area, is commonly observed and markedly diminishes their antimicrobial efficacy. Consequently, a chemical pretreatment of the AgNPs surface is needed prior to gel formation.[11]

Compared to the widely studied macromolecular gels, supramolecular gels have attracted substantial attention because of their promising applications in biotechnology and bioengineering. Supramolecular hydrogels are based on low molecular weight gelators (LMWGs) that undergo self-assembly, forming hierarchical nanostructures through non-covalent interactions, thereby establishing a three-dimensional (3D) entangled network in aqueous environments.[12-14] Seminal studies have reported the use of supramolecular hydrogels for the growth of metal NPs, however, these endeavors still relied on the employment of toxic reducing agents or external stimuli such as photoreduction.[15,16]

Carbohydrate-based gelators have been attracting tremendous attention since carbohydrates are biosourced, abundant, renewable, biodegradable and non-toxic, filling the criteria of “green” industry. Carbohydrates not only act as hydrophilic groups but also contain

multiple hydroxyl groups that serve as hydrogen-bonding sites involved in the 3D-network formation. Moreover, as already mentioned, the open-chain aldehyde form of carbohydrates could act as reducing agent by transferring electrons to another species, *e.g.*, to Ag^{+}, producing AgNPs.[10]

Therefore, the originality of this work consists in creating a carbohydrate-based supramolecular hydrogels constituted of reducing carbohydrate derivatives enabling intrinsic reduction of silver ions towards antibacterial AgNPs stabilized into the 3D entangled self-assembled network (Illustrated in **Figure 1**). To the best of our knowledge, there is no reports on the *in situ* synthesis of AgNPs utilizing native reducing-end carbohydrate-based supramolecular hydrogels. To achieve this purpose, novel reducing end glucosamine-based gelators have been synthesized, capitalizing on the site-selective modification of protecting group-free carbohydrates on the amino function of glucosamine with *N,N'*-disubstituted barbituric acid derivatives. The selection of substituents on the barbituric ring has been meticulously tailored to promote gel formation through cooperative interactions, encompassing hydrogen bonding, π-π interactions, and hydrophobic interactions. Ultimately, *in situ* formation of AgNPs@supramolecular hydrogels has been performed and have demonstrated antimicrobial activity, thereby addressing a crucial aspect of their potential applications.

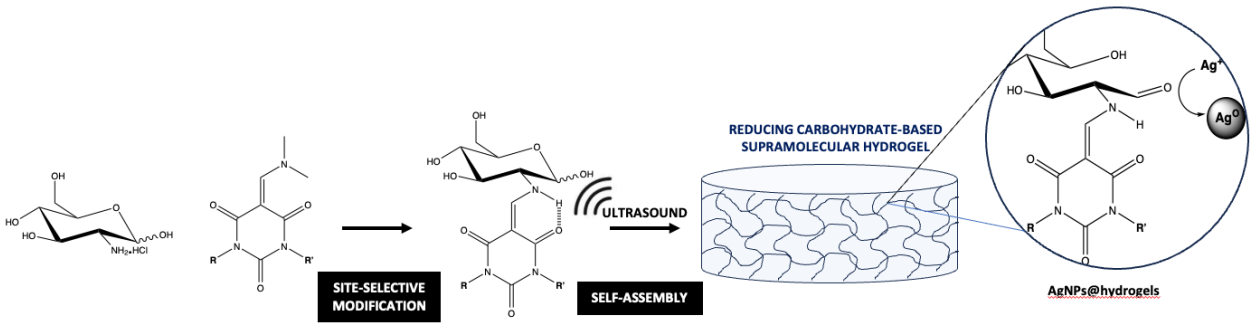

Figure 1. Schematic illustration of a reducing carbohydrate-based supramolecular hydrogel formed by self-assembly enabling *in situ* formation of AgNPs

2. RESULTS AND DISCUSSION

2.1 Carbohydrate-based hydrogelator design. To achieve our objective, the synthesis of free reducing end carbohydrate-based hydrogelators is required. Hydrogelators, as previously indicated, are amphiphiles encoding different forms of non-covalent interactions. The preparation of glyco-hydrogelators necessitates the introduction of a hydrophobic segment (alkyl or aromatic group) by covalently attaching to one of the chemical functions of the hydrophilic carbohydrate, except on the anomeric position. It is worth noting that the majority of carbohydrate-based hydrogelators are currently amphiphilic glycoconjugates that have been altered at the reducing end position because of convenient synthetic reasons.[17,18] In our work, we prioritize chemo- and site-selective modifications of carbohydrates since they prevent the need for time-consumption and laborious protection/deprotection steps.

Naturally occurring D-glucosamine, that can be extracted from crustacean exoskeletons and fungal mycelial mats, has a noteworthy advantage due to its amino-group at the C2 position which exhibits heightened reactivity compared to hydroxyl group. A previous publication reported that D-glucosamine hydrocholoride reacted chemo-selectively at amino function position with 9-fluorenylmethyl chloroformate which generated supramolecular hydrogels with self-assembled nanofiber structures.[14] If this strategy is definitively interesting, it is limited to a few structures depending on commercially available aryl chloroformate derivatives. Our research group initially proposed barbituric acid derivatives as a versatile and efficient chemical platform for the protecting-group-free modification of carbohydrates at the anomeric position, facilitated by Knoevenagel condensation in water.[19-21] The barbituric acid chemical toolbox provides

remarkable structural and functional diversity which is conducive to diversity-oriented synthesis of (neo)glycoconjugates. Noteworthy, 1,3-dimethyl-5-[(dimethylamino)methylene] 2,4,6 (1*H*, 3*H*, 5*H*)-trioxopyrimidine (DTPM reagent), a 5-substituted barbituric derivative, has been developed to readily protect the amino function of carbohydrates in MeOH.[22] Therefore, based on our previous works, we originally proposed *N,N'*-disubstituted barbituric acid derivatives as hydrophobic segments that could react with the amino function of D-glucosamine. Following this strategy, the potential glyco-hydrogelators will possess a free reducing end, serving as the reducing site, allowing us to prepare *in situ* synthesis of antimicrobial AgNPs@supramolecular hydrogel composites. *N,N'*-disubstituted barbituric acid derivatives incorporating aromatic groups (R1, R2) have been selected because of π-π and/or CH–π interactions that are well-known to promote self-assembly (shown in Scheme 1).[23]

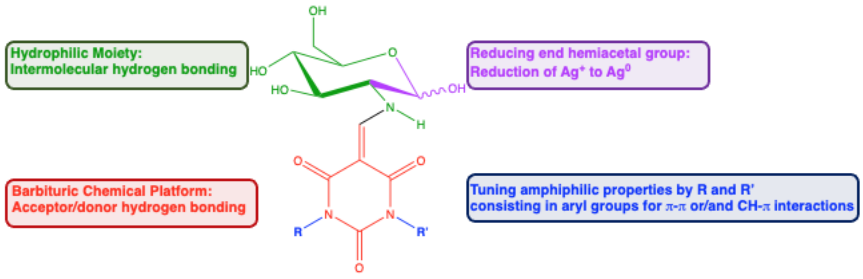

Scheme 1. Design of the chemical structure of reducing-end 2-deoxy-2-*N*-(*N,N'*-disubstituted barbituryl)glucosamine hydrogelators

In order to achieve a proper hydrophilic-lipophilic balance (HLB) for exhibiting hydrogelation, we synthesized a series of potential 2-deoxy-2-*N*-(*N,N'*-disubstituted barbituryl)glucosamine hydrogelators (**1d** to **5d,** in Scheme 2). Firstly, the activated *N,N'*-disubstituted barbituric acid derivatives were synthesized in three steps. The primary arylamines reacted, in *t*-BuOH, with *N,N'*-carbonyl diimidazole at 40 °C leading to symmetrical ureas **1a**, **3a** and **5a** (Step (i), in

Scheme 2) that were easily recovered by filtration at the end of the reaction. Besides, the unsymmetrical urea **2a** and **4a** were obtained by reacting isocyanate derivatives with primary amines in dry DCM at room temperature. Then, after dilution with dry DCM, the urea derivatives were cyclized with malonyl chloride at 40 ℃ to readily afford the corresponding *N,N'*-disubstituted barbituric acid derivatives (Step (ii), in Scheme 2). Next step is the Knoevenagel condensation with DMF at 90 ℃ in acetic anhydride, to give the final activated *N,N'*-disubstituted barbituric acid derivatives. (Step (iii), in Scheme 2). The yield of compound **3c** was too low (28%) by following this way, so compound **3b** was rather reacted with *N,N*-dimethylformamide dimethyl acetal, in dry $HCCl_3$ at rt, significantly increasing the yield of compound **3c** (60%). Finally, the expected glyco-hydrogelators (**1d** to **5d**) were synthesized (the detailed synthesis were shown in Supporting Information) by coupling the activated *N,N'*-disubstituted barbituric acid derivatives with D-glucosamine hydrochloride at rt in MeOH and in presence of $NaHCO_3$ (Step (iv), in Scheme 2). The structures of compounds from **1d** to **5d** are shown in Scheme 2 and were well characterized by ^{1}H and ^{13}C NMR, mass spectrometry and FT-IR (See Supporting Information, Figures S1–S32).

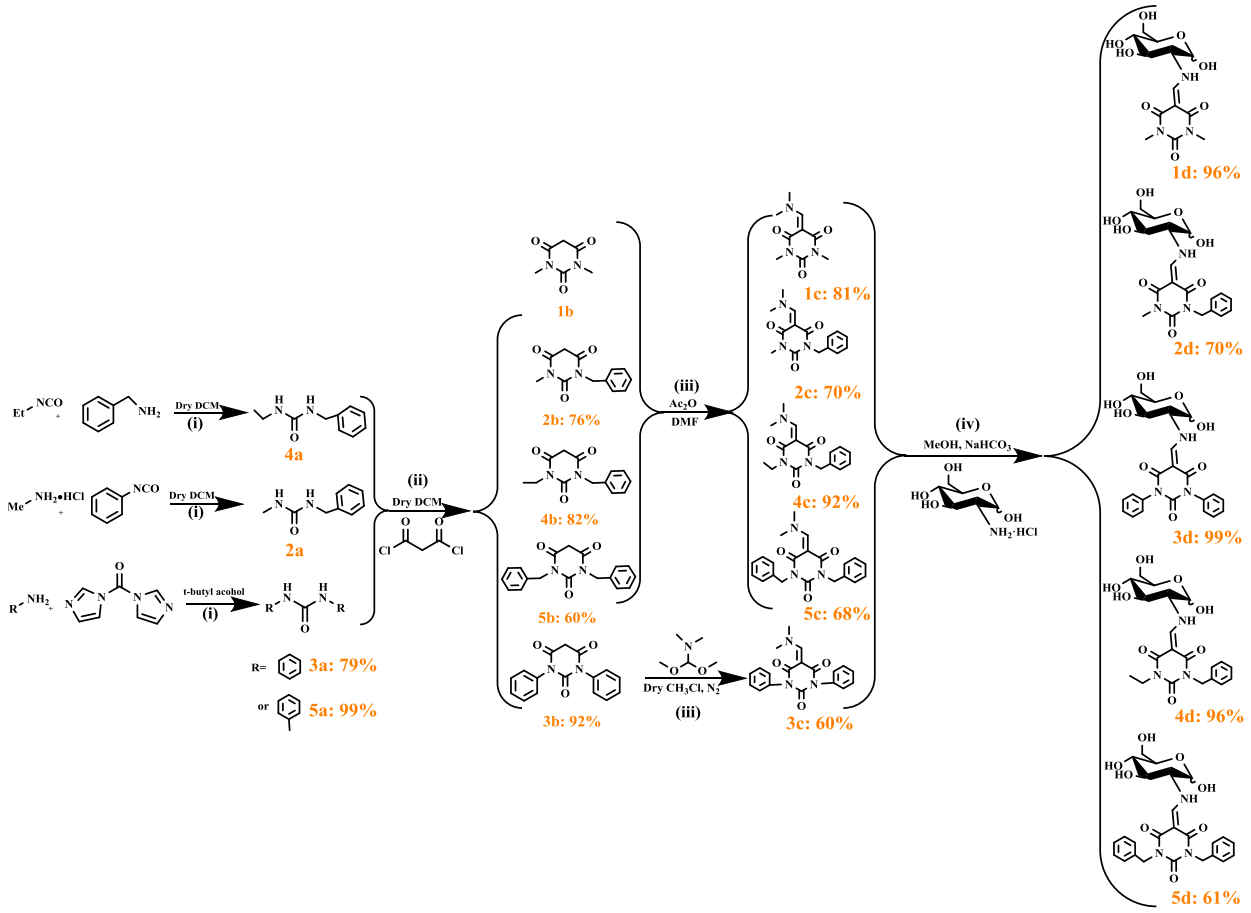

Scheme 2. The 4-steps synthetic route towards reducing-end glyco-hydrogelators (**1d** to **5d**)

2.2 Hydrogelation studies and physical-chemical characterization of the hydrogel. In order to get hydrogelation properties, the prerequisite is that compounds have to be non-soluble in water at rt and to provide a clear homogeneous solution after heating. Next, when the solution is allowed to cool down, a self-standing gel, upon tube inversion, has to be observed. And if the gelation is observed, we decrease the weight concentration in order to determine the minimal gel concentration (MGC). The gelation tests were undertaken and unfortunately, the carbohydrate derivatives **1d** to **5d** at 5 wt.% failed to form a gel in water following the heating/cooling cycle. However, we serendipitously found that compound **4d** (5 wt.%) exhibited a self-supporting gel capability in water upon ultrasound irradiation (0.56 W cm^{-2}, 37 kHz, 25 °C) for 30 min and

vortexing for better dispersion. Afterwards, we screened out other compounds (**1d**, **2d**, **3d**, **5d**) in the same way, but all of them cannot generate hydrogel when they were sonicated even for 120 min and left to rest for a long time. The concentration of compound **4d** was decreased to 4 wt.%, 3 wt.%, 2.5 wt.% and 2 wt.%, all of them can generate hydrogel except for 2 wt.% in the same way above. Therefore, hydrogelator **4d** has a minimal gelation concentration (MGC) of 2.5 wt.% after 2 hours of rest. The inability to obtain sonication-induced hydrogels for compound **3d**, that differs only from a methylene carbon, revealed the utmost importance of the delicate HLB impacting on the solubility and, ultimately, on gelling properties. This emphasizes once again the difficulty of predicting the right structure to obtain a hydrogelator and that the screening of a series of amphiphiles remains needed.

Only recently, ultrasound has been found to be an external physical stimulus to initiate the self-assembled fibrillar networks of gelators in a given solvent.[24-28] The force of ultrasound was thought to rearrange the aggregation of molecules by cleaving self-locked intramolecular hydrogen bonds or π - π stacking to form interlocked structures through intermolecular interactions. To gain insight information on the supramolecular interactions present **4d**, ^{1}H NMR (Figure S34) and FT-IR (Figure S33) experiments were carried out. Indeed, enamines derived from D-glucosamine and β-diketones are well-known to establish an intramolecular hydrogen bond between N-H from sugar and C=O from β-diketone.[29] The FT-IR spectroscopy (Figure S33) of as-prepared **4d** showed a low stretching-frequency at 1631 cm^{-1} that was attributed to C=O stretching mode vibration of barbituric ring involved in intramolecular hydrogen bonding interactions. Indeed, the carbonyl absorptions for barbituric derivatives are usually observed around 1750 cm^{-1}.[30,31] For the gel state induced by sonication, C=O band was splitted into two bands at 1650 cm^{-1} and 1625 cm^{-1} that were characteristics of different modes of intermolecular

hydrogen bonding interactions. The freeze-dried hydrogel showed the same FT-IR spectra than the as-prepared solid compound **4d** revealing a disruption of the intermolecular hydrogen bonding by this process. Moreover, the chelate structure was further demonstrated by the two multiplets at low field (δ 10.20 ppm) assigned to the N-H proton for a solution in DMSO-d_6 (Figure S34). The large paramagnetic shift is due to the presence of the strong intramolecular hydrogen-bond, and the splitting to the presence of two coexisting rotational isomers (rotamers **I** and **II** in Scheme 3) due to the asymmetry of the barbituric ring and were estimated thanks to the proton integration to be in a ratio of 1:1. This equimolar ratio indicates that no rotamer is favored likely because no steric hindrance occurs either with benzyl or ethyl group. In support of these experimental data, we can reasonably claim that our **4d** hydrogelator originally exists in a deactivated form, because of the self-locked intramolecular bond -C=O----H-N-, and that ultrasound allows breaking of this bonding leading to an activation of **4d** conducive to intermolecular *H*-bonding essential to the formation of a three-dimensional network and ultimately to the formation of a supramolecular hydrogel. This mechanistic pathway is illustrated in the following Scheme 3.

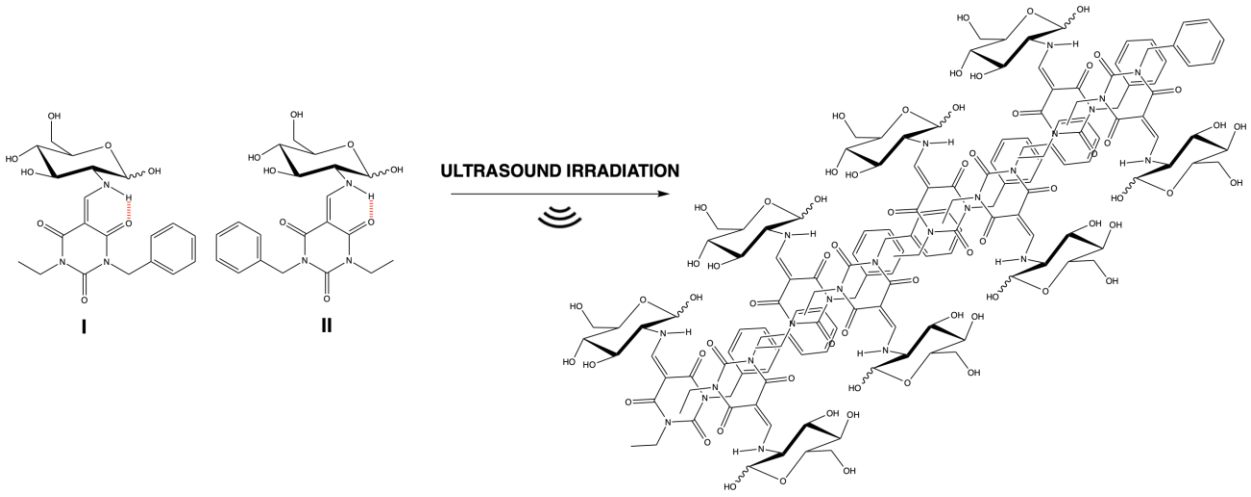

Scheme 3. Ultrasound-induced breaking of self-locked intramolecular hydrogen bond of **4d** rotamers (**I**) and (**II**) to activate supramolecular polymerization

The photographs of the opaque gels formed with compound **4d** at 4 wt.% are shown in Figure 2. We demonstrated that a thermoreversible hydrogel **4d** could be obtained after heating up to almost 100 ℃ without achieving full solubilization (Figure 2A) and then a new round of sonication. While, a complete solubilization did not allow gelation even after ultrasound irradiation. It could be concluded that the residual hydrogel could act as seeding growth for promoting the self-assembly and ultimately hydrogel formation.

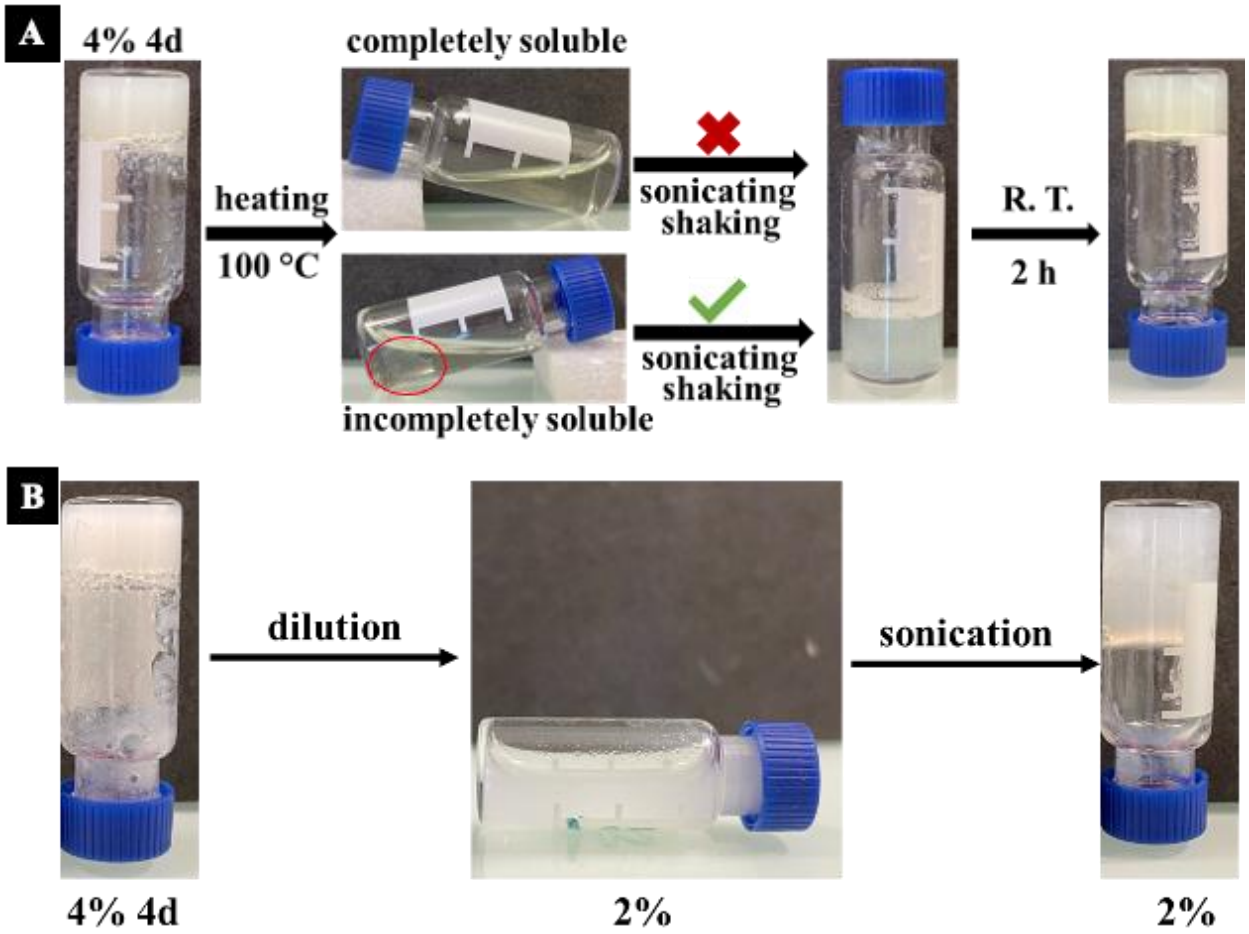

Figure 2. Representative images of **4d** hydrogels A) showing thermoreversible properties after partial dissolution and B) subjected to dispersion from 4 wt.% to 2 wt.% then sonication

Besides, hydrogel **4d** at 4 wt.% was broken by vigorous mixing by vortex, therefore mechanically disrupting the hydrogel network, and then some deionized water was added for reaching a concentration of 2 wt.%, below the previously determined MGC value of 2.5 wt.%. The dispersed solution was sonicated for 10 min and after allowing time for recovery (12h), the hydrogel network was reestablished as assessed by vial inversion method (Figure 2B), illustrating the self-healing behavior. When it was diluted to 1.5 wt.%, it cannot form hydrogel even after 1 week of rest. Besides, hydrogels **4d** at 4 wt.% and 5 wt.% were broken by vortex and then were transferred to other two vials with syringe (scale: 10 mL, needle: 1.1 * 38 mm). Hydrogel recovery was observed, without any other treatments, after 2 h for 4 wt.% and in a shorter time of 3 min for 5 wt.% (Figure S35). The gelation speed increased with increasing of the hydrogelator concentration. All these experiments clearly indicate the self-healing capability or thixotropy of the supramolecular hydrogel **4d**. Thixotropic shear-responsive self-healing behavior is an important feature for biological applications such as injectable sustained-release drug delivery systems.

The rheological evaluation was performed to gain insights into the viscoelastic and mechanical behavior of hydrogel **4d**. Figure 3A determined the correlation between G' and G" for hydrogel **4d** at 5 wt.% and 8 wt.% concentration with respect to strain. The linear viscoelastic region (LVE region) revealed that G' surpasses G" by an order of magnitude, for both concentrations. The critical strain values for hydrogels with 8 wt.% and 5 wt.% wt. is 0.96% and 13.9%, respectively. Low-concentration hydrogel had a higher critical strain, resulting in a broader LVE, showing that hydrogel with 5 wt.% had better resistance to an applied force before deformation. On the other hand, high-concentration hydrogel had the lowest critical strain and greater G' value, maybe due to low mobility chains or the formation of more tiny self-assembled

structures in hydrogel which probably promote water migration. Beyond these values, G' and G" markedly decreased, causing the cross-point G' = G", indicating the critical transition point between the gel and the liquid state. This led to permanent deformation in the 3D network.

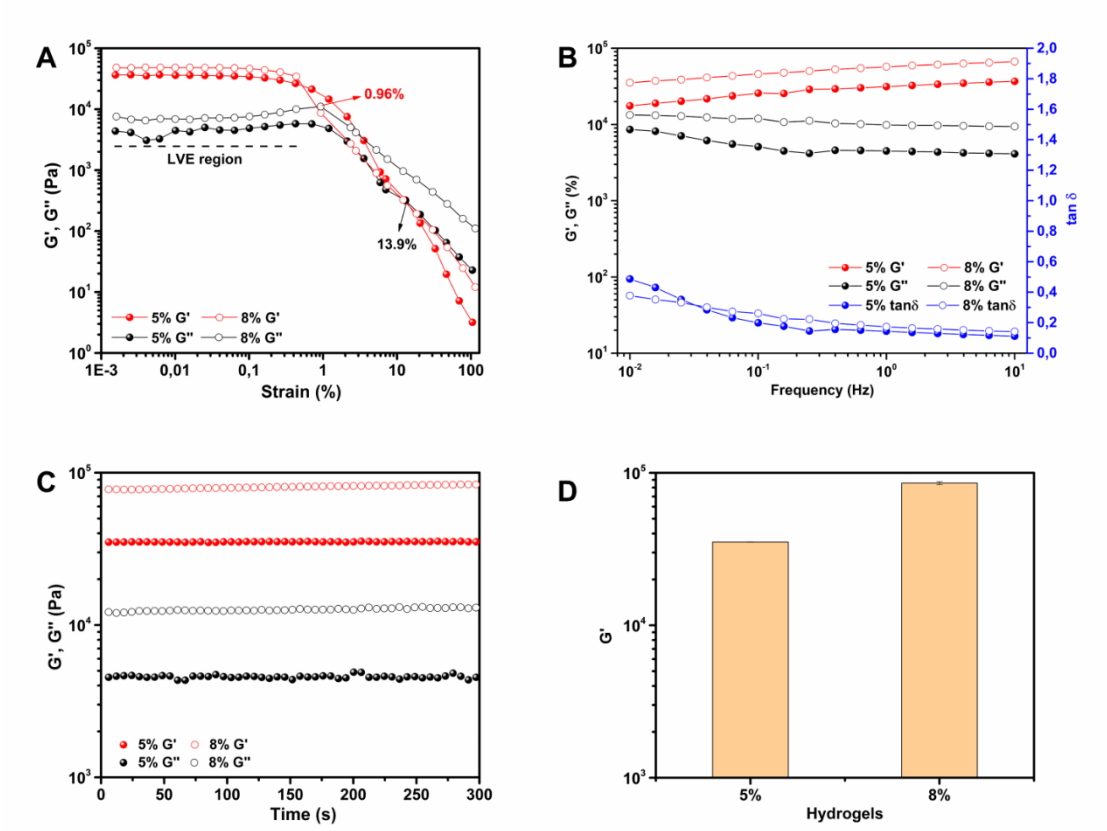

Figure 3. Storage modulus (G', sphere) and Loss modulus (G", star) *vs* strain (A) and frequency (B) curves of hydrogel **4d** at different concentration, (C) the G vs time at different concentration, (D) the comparison of G" vs concentration.

To obtain further insights, a frequency sweep was carried out, which revealed the relationship between G' and G" of hydrogel **4d** at different concentrations *versus* frequency, as shown in Figure 3B. Throughout the frequency spectrum, the G' value consistently exceeded that of G", indicating an apparent elastic response and a permanent, solid-like behavior. The frequency dependence of G' and G" values was low, with only slight increases for G' and slight decrease for

G" observed as the frequency increased. This suggests that the network does not exhibit complete elasticity, which results in sluggish tough recovery following stress application. The increase in concentration generated an increment in the G' value, meaning that the 8 wt.% hydrogel exhibits greater resistance to deformation and a higher network gel strength than its 5 wt.% counterpart. These outcomes are consistent with the strain sweep outcomes mentioned previously. Notably, all the hydrogels exhibited a tan δ (G"/G') value greater than 0.1, indicating solid gels. The G' and G" values has been constant for 300 s (shown in Figures 3C and 3D) and G' value of 8 wt.% was higher than that of 5 wt.%, still demonstrating the hydrogel exhibits solid-like behavior and better mechanical properties.

The TEM photos of hydrogel **4d** at 3 wt.% (A), 4 wt.% (B), 5 wt.% (C) are shown in Figure 4 and revealed an entangled bundles of individual **4d** nanofibers with several micrometers in length and rather uniform diameters of about 10 nm at 3 wt.% and 4 wt.%. Bundles of nanofibers in hydrogel at 5 wt.% has been observed (Figure 4C) owing to the higher concentration. In addition, the morphology of self-assembled structures in hydrogel at 2 wt.% obtained by dispersion from hydrogel at 4 wt.% is still fibrous nature (Figure S37).

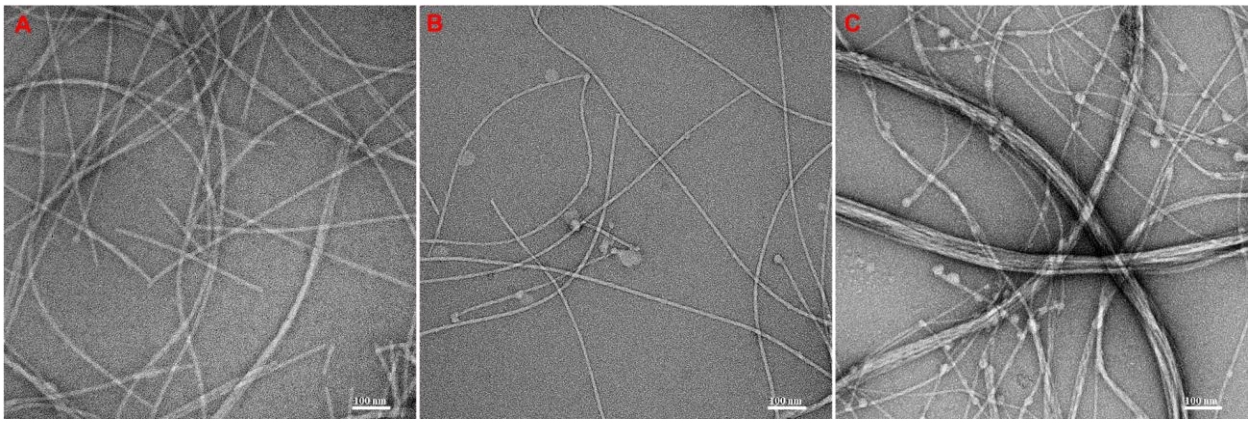

Figure 4. The TEM photos of **4d** hydrogels at 3 wt.% (A), 4 wt.% (B) and 5 wt.% (C) (Scale bar = 100 nm).

2.3. *In situ* preparation of AgNPs@hydrogel and AgNPs characterization. TEM images obtained from *in situ* AgNPs@hydrogel composites (Table S1) are shown in Figure 5. First, TEM images revealed still a fibrous gel network during the *in situ* preparation of AgNPs (Figures 5B and 5C) comparatively to the absence of silver salts (Figure 5A). The spherical micelles of **4d** observed in Figure 5C is mainly due to the dilution effect during the preparation of TEM grid. Second, black nanoparticles appeared in Figure 5B and Figure 5C corresponding to AgNPs formed *via* the reduction of silver ions with reducing glucosaminylbarbiturate hydrogelators. The average diameters of the spherical particle size of AgNPs are 9.7±2.4 nm at 0.37 mM and 17.2±4.1 nm at 0.74 mM, indicating that the size of AgNPs can be controlled by adjusting the concentration of silver ions. The size and aggregation state of AgNPs remained stable at least for 1 month, which could be assigned to the interaction of carboxylate groups oxidized from aldehyde groups during the reduction of silver ions with the surface of AgNPs[32-34] and the physical isolation resulting from 3D networks of hydrogel. Interestingly, the AgNPs were mainly located along the length of the nanofibers, assuming that the peripheral carbohydrates in the nanofibers served as nucleation and reactive sites during the silver reduction. Here, we validated our proof-of-concept consisting in *in situ* synthesis of AgNPs using reducing carbohydrate-based hydrogelators as stabilizing agent and reducing sites, avoiding the need for external reducing agent, nucleating agent, stabilizer and other additives.

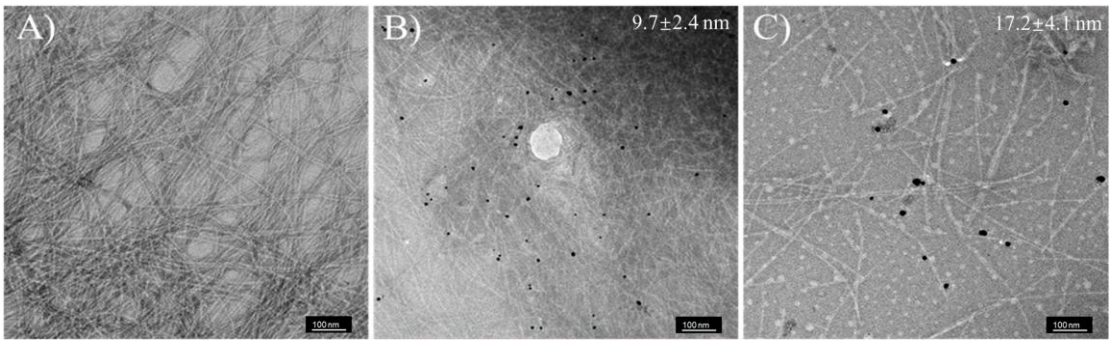

Figure 5. TEM photos of (A) hydrogel **4d** at 4 wt.%, and with (B) AgNPs at 0.373 mM and (C) AgNPs at 0.743 mM

The optical characterization of the AgNPs produced by our reducing glucosaminylbarbiturate hydrogelator **4d** was studied by UV–vis spectroscopy (Figure 6). Since the gels were opaques (Figure S36), the absorption spectra were recorded over time in a diluted solution of hydrogelator **4d** with a concentration of 5.734 mM and Ag^{+} ions with a concentration of 0.186 mM (Figures 6A and 6B) corresponding to a molar ratio 30:1. The formation of AgNPs was further evident from the sharp surface-plasmon resonance (SPR) peak at 422 nm. The time-dependent investigation on the growth of the SPR peak showed that *in situ* synthesis of AgNPs was successfully carried out (Figures 6B and 6C). In addition, the SPR peak is a single peak and become sharper over time, indicating the formation of sphere-like AgNPs, as already observed by TEM images.[35] In addition, the absorbance intensity in the region of 600-700 nm increased with ageing of the sample indicating the size growth or aggregation of silver nanoparticles over time.

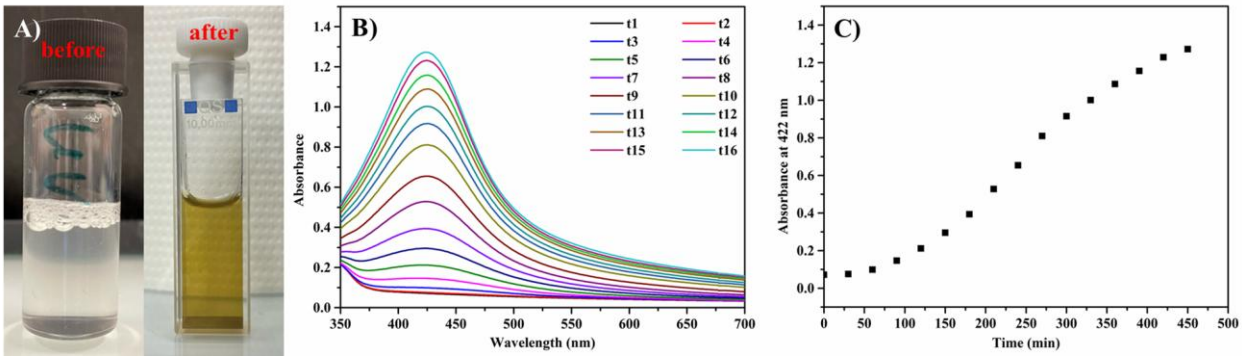

Figure 6. A) Photograph images of the solution of hydrogelator **4d** (5.734 mM) mixed with Ag^{+} ions (0.186 mM) at t0 (before) and at t16 hours (after); B) UV–vis absorption spectra of the solution at different time intervals during the AgNP growth (in hours) from t1 to t16; C) Intensity of SPR band (422 nm) as a function of reaction time.

2.4. Antibacterial effect of the AgNPs@hydrogel composite. In biomedical applications, there is a huge interest in creating materials or coatings with antimicrobial properties, particularly against multi-drug resistance bacterial strains.[36] Because of its low toxicity, biocompatibility, high surface to volume ratio, oxidation resistance and chemical stability, AgNPs have already been used as antibacterial and antimicrobial coating for medical devices to prevent implant-related infections.[37] Therefore, we investigated the antibacterial properties of the composite AgNPs@hydrogel against both Gram-positive (*Bacillus subtilis* (*B. subtilis*) and *Staphylococcus aureus* (*S. aureus*)) and Gram-negative (*Pseudomonas aeruginosa* (*P. aeruginosa*)) pathogenic bacterial strains (Table S2). The inhibition zones were determined and collected in mm for each organism and shown in Figures 7, S38 and S39 and Table S3. First, it is noteworthy that hydrogel **4d** without AgNPs exhibited a selective antibacterial effect to bacteria *B. subtilis* and the concentration of hydrogel (4 wt.% or 8 wt.%) has no impact on the inhibition effect based on the inhibition zone diameters. This antibacterial effect of the hydrogelator **4d**, that is a carbohydrate-based amphiphile, was not surprising since surfactants are known to disrupt the bacterial cell membranes[38,39] even if the selective antibacterial effect toward only *B. subtilis* is not understood. The presence of AgNPs in AgNPs@hydrogel composites displayed an enhanced and significant antibacterial activity towards both Gram-positive bacteria (*B. subtilis* and *S. aureus*) and, even better for Gram-negative bacteria (*P. aeruginosa*). It is noteworthy that AgNPs@hydrogel 4 wt.% composite has better antibacterial effect than that with AgNPs@hydrogel 8 wt.% composite, which can be assigned to a more porous entangled 3D network which accelerate the diffusion of silver ions out of the hydrogel improving their antibacterial effect around the surrounding surface.[40] Based on the antibacterial effect of

AgNPs@hydrogel against pathogenic strains, it can serve as potential and efficient antibacterial green material.

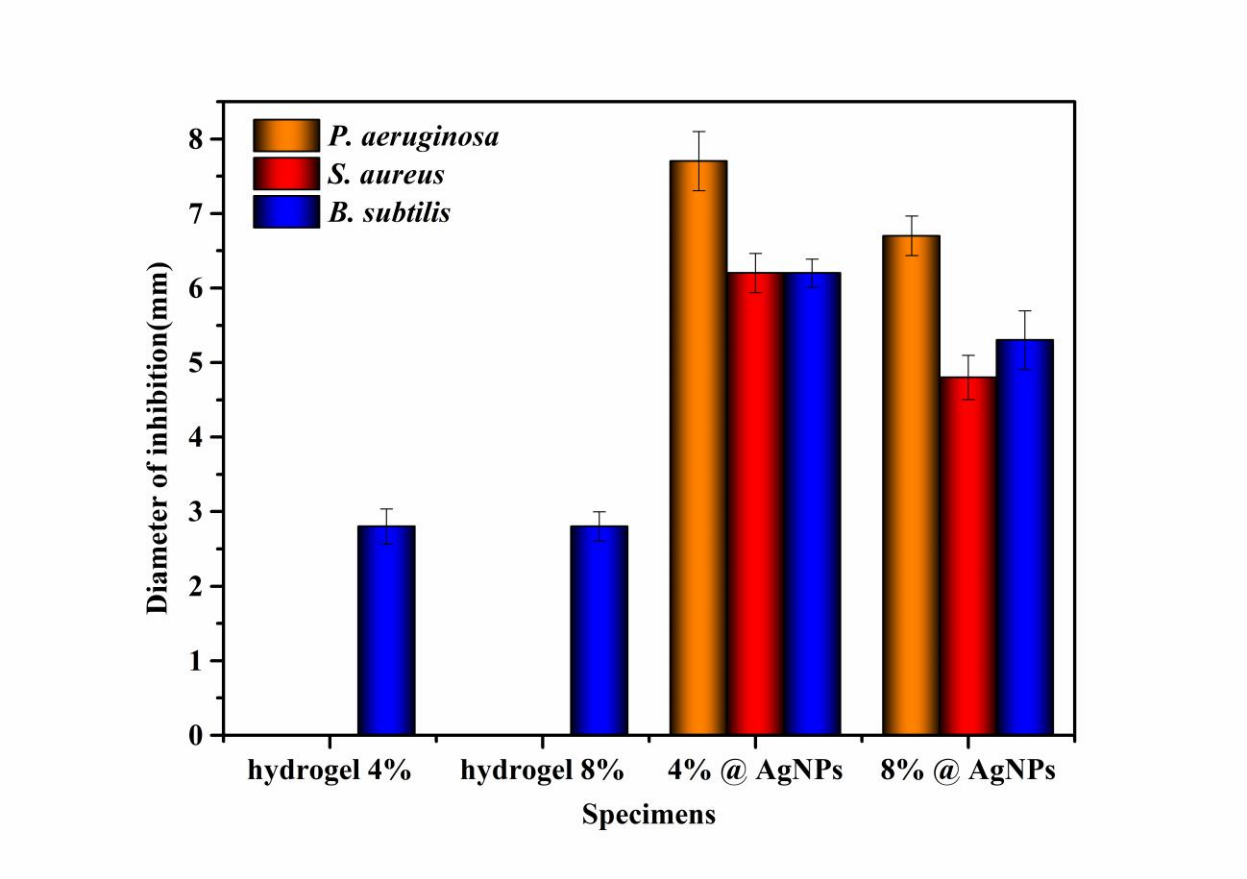

Figure 7. Kill zone diameters for **4d** hydrogel and AgNPs@hydrogel of varying bacteria.

3. CONCLUSIONS

In summary, we report a single step synthesis of a new family of reducing glucosamine-based hydrogelators by reacting chemo-selectively the amino function of protecting group-free glucosamine with activated barbiturate derivatives that served as a modular chemical platform. An ultrasound-driven glucosaminylbarbiturate-based supramolecular hydrogel has been successfully achieved where ultrasound activation was thought to cleave the intralocked hydrogen bonding in the hydrogelator **4d** to reconfigure towards intermolecular interactions needed for the establishment of a 3D network. Subsequently, AgNPs were formed within the

supramolecular hydrogel by *in situ* reduction of silver ions in one-pot, in which the free reducing end of carbohydrate-based gelators acted as reducing, nucleating and stabilizing sites preventing the need for extra toxic reducing agents and stabilizers. Finally, the AgNPs@hydrogel composites were demonstrated to have antibacterial effects against both Gram-positive and Gram-negative pathogenic bacterial strains. Owing to the ease of fabrication and antibacterial performance, the antibiotic-free AgNPs@hydrogel should have great potential in broad spectrum antibacterial "green" soft material for biomedical applications.

4. EXPERIMENTAL SECTION

4.1. General Methods. All chemicals were bought from Sigma-Aldrich (Saint Quentin Fallavier, France) and were used as received. The progress of the reactions was monitored by thin layer chromatography (TLC) using silica gel 60 F254 precoated plates (Merck). Spots were visible using UV light or by charring with solution of H_2O/MeOH/H_2SO_4 (225/225/15, v/v/v) or by staining with $KMnO_4$ solution. Column chromatography was conducted by manual flash chromatography (wet-packed silica, 40–63 μm, VWR Chemicals). The IR spectra of samples were recorded by transmission from 400 to 4000 cm^{-1} (4 scans resolution 2) using a PerkinElmer spectrometer. Bruker Advance DRX400 (400 MHz) and (100 MHz) spectrometers were utilized to record nuclear magnetic resonance spectra ^{1}H NMR and DEPT135 ^{13}C NMR of specimens, respectively. Mass spectra (ESI-MS) were carried out using on an Esquire 3000 spectrometer from Bruker. High-resolution mass spectra (HRMS-ESI) were conducted on a Waters Xevo® G2-S QTof. Rheological properties of hydrogels were performed on a DHR3 rheometer (TA instruments, New Castle, DE) instrument. TEM images: the specimens were observed with a JEOL JEM-2100 Plus microscope operating at 200 kV and images were recorded with a Gatan Rio 16 digital camera. UV-Visible absorption spectra were recorded on JASCO Chromatography

and Spectroscopy (V-770, D10656181). The rheological analysis of oleogels was performed on a DHR3 rheometer (TA instruments, New Castle, DE) instrument. Optical microscope images were recorded with an Olympus SC50 digital camera operated by the stream acquisition software in a Zeiss Axiophot 2 microscope equipped with polarized light. *Staphylococcus aureus* strain Wichita (ATCC29213) was a gift from Yvan Caspar; *Bacillus subtilis* strain 168 (ATCC 23857) was a gift from Cécile Morlot; *Pseudomonas aeruginosa* strain PA14 (Rahme et al, 1995, Science vol268) was a gift from Sigolène Lecuyer.

4.2. General procedure for the synthesis of amphiphilic glucosaminyl barbiturates (1d-5d). The activated *N,N'*-disubstituted barbituric acid derivative (**1c, 2c, 3c** or **4c**, 2 mmol) reacted with D-glucosamine hydrochloride (2.4 mmol) at room temperature in methanol (10 mL) and $NaHCO_3$ (4 mmol) was added into the mixture. The reaction was confirmed by TLC (Acetonitrile/water, 9/1 v/v). The solvent was concentrated by rotavapor and the crude product was directly purified via flash column chromatography to give in high yields **1d**, **2d**, **3d**, **4d** or **5d**.

4.3. Preparation of supramolecular hydrogels. All of these compounds (25 mg) were added into individual vials, then 500 μL of deionized water was added to give a final weight concentration of 5 wt.% (w/v). For the stimulus of ultrasound, the vials were placed into an ultrasound cleaner (90 W, 50 / 60 Hz, temperature should be kept in the range from 25 ℃ to 35 ℃) for sonicating about 30 min and then vortexing necessary to complete dispersion. After that the vials were put at room temperature for gel formation. We decreased the weight concentration in order to determine the minimal gel concentration (MGC) when the gelation was observed. The states of the phase were confirmed if these two criteria were met: (1) by visual observation; (2) when inverted, sample did not flow.

4.4. *In situ* preparation of AgNPs@hydrodrogel composites. Compound **4d** (20 mg) was added into several vials, then defined volumes of deionized water and Tollens' solution was sequentially added (Table S1). The vials were covered by aluminum foil to avoid light exposure. Afterwards, these vials were put into the ultrasound cleaner (90 W, 50 / 60 Hz, temperature should be kept in the range from 25 ℃ to 35 ℃) for sonication. Finally, all of these vials were placed in darkness at room temperature to afford AgNPs@hydrogel composites (Figure S36).

4.5. Antibacterial tests procedure. 1 mL of LB (Lurie Broth) medium and 1 bead of *P. aeruginosa* or 1 mL of LB medium and 1 bead of *B. subtilis*, or 1 mL of BHI (Brain-Heart Infusion Broth) and 1 bead of *S. aureus Wichita* were cultured at 37 °C at 300 rpm for 16 h. Then *P. aeruginosa* (OD = 2.4), *B. subtilis* (OD = 6) and *S. aureus* (OD = 14) were diluted to OD = 0.001 in sterile PBS. 75 µL of these diluted bacteria were spread on LB (*P. aeruginosa and B. subtilis*) or BHI (*S. aureus*) agar plates (diameter = 850 mm). Around 25 mg of specimens (hydrogel or AgNPs@hydrogel composite) were directly deposited on the surface of dishes. Spatulas were cleaned with paper tissue and then EtOH 90% to avoid cross contamination with hydrogels and with bacteria. On top of a sterile filter paper, 2 µg of ciprofloxacin were put on the dishes as control for the three bacteria species. Plates were then incubated overnight at 37°C.

The **error bar** was obtained from standard deviation:

$$\delta(\mu) = \sqrt{\frac{1}{N}\sum_{i=1}^{N}(X_i - \mu)^2}$$

X_i values are obtained by detecting the diameters of inhibition area, 5 times for each inhibition area. Every specimen has 3 inhibition area.

µ value is the average value for each specimen.

Specimens	***P. aeruginosa***	**Y error**	***S. aureus***	**Y error**	***B. subtilis***	**Y error**
hydrogel 4 wt.%	0		0		2.8	0.2368

hydrogel 8 wt.%	0		0		2.8	0.1963
AgNPs@4%	7.7	0.3973	6.2	0.2637	6.2	0.1893
AgNPs@8%	6.7	0.2638	4.8	0.2971	5.3	0.3942

4.6. Transmission Electron Microscopy. Since the opaque gels could not be directly observed by TEM, a small piece of gel was put onto carbon coated grid and dispersed with a drop a water. A drop of negative stain with 2 wt.% uranyl acetate was added, and the excess of stain was removed to get a very thin film and let it dry at room temperature for TEM images. The specimens were observed with a JEOL JEM-2100 Plus microscope operating at 200 kV and images were recorded with a Gatan Rio 16 digital camera.

4.7. Rheological measurements. To check the mechanical properties of the hydrogels, the rheological analysis of hydrogel **4d** at 5 wt.% and 8 wt.% were carried out on a DHR3 rheometer (TA instruments, New Castle, DE) instrument, equipped with a water cycle temperature controller, fixing a temperature of 20 °C. A geometry cone-and-plate 20 mm in diameter and 104 μm in the gap was used for the measurements. Samples were carefully applied to the plate, minimizing sample shearing. The amplitude sweeps within the strain range of 0.001-100% were applied to determine the linear viscoelastic region at a frequency of 1 Hz. The viscoelastic properties of the solutions were evaluated by the oscillatory frequency sweep experiments carried out with a constant strain while the frequency increased in a 0.01-10 Hz range (0.04% of strain). The oscillation time was performed with a constant strain of 0.04% and 1 Hz of frequency. The storage modulus and the loss modulus G´´ of the sample were recorded as a function of time. The measurements were repeated three times to ensure reproducibility, with the average data shown. The rheological teat of hydrogels **4d** at 5 wt.% and 8 wt.% has been performed at the strain of 0.1% and frequency of 1 rad/s.

4.8. UV-visible absorption spectra of AgNPs in solution. To further investigate the formation of AgNPs, hydrogelator **4d** (5 mg) was added into a vial with 325 µL of deionized water and then the mixed solution was sonicated for 10 min at room temperature. Afterward, 175 µL of Tollens' solution and 1.5 mL of deionized water were added resulting in afinal concentration of Ag^+ 0.186 mM. Finally, the solution was transferred into a quartz cuvette. UV-vis spectra were recorded every 30 min using a 1 mm path length cuvette. The cuvette was kept closed during the test to prevent evaporation.

ASSOCIATED CONTENT

Supporting Information

The Supporting Information is available free of charge at https://pubs.acs.org/doi/... .

Experimental sections; NMR spectra; Pictures of self-healed hydrogels; Preparation of Tollens' solution and AgNPs@hydrogel composition with corresponding images; TEM images of diluted hydrogels; Polarized optical microscopy of hydrogels at 5 wt.% and 8 wt.%; Images of inhibition zones on petri dishes and compositions of studied AgNPs@hydrogels with table of inhibition zone diameters in triplicate.

AUTHOR INFORMATION

Corresponding Author

Sami Halila – Department of Self-Assembly of Glycopolymers, Univ. Grenoble Alpes, CNRS, CERMAV, 38000 Grenoble, France; orcid.org/0000-0002-9673-1099; Email: sami.halila@cermav.cnrs.fr

Authors

Bing Chen – Department of Self-Assembly of Glycopolymers, Univ. Grenoble Alpes, CNRS, CERMAV, 38000 Grenoble, France

Elizângela Hafemann Fragal – Department of Self-Assembly of Glycopolymers, Univ. Grenoble Alpes, CNRS, CERMAV, 38000 Grenoble, France; orcid.org/0000-0002-2081-1340

Eric Faudry – CEA, INSERM, CNRS, Bacterial Pathogenesis and Cellular Responses, University Grenoble Alpes, UMR 1036/ERL 5261, 17 avenue des Martyrs, 38054 Grenoble, France; orcid.org/0000-0001-9958-6029

Present Addresses

† **Elizângela H. Fragal** – Univ. Grenoble Alpes, CNRS, Grenoble INP (Institute of Engineering Univ. Grenoble Alpes), LRP, 38000 Grenoble, France

Author Contributions

The manuscript was written through contributions of all authors. All authors have given approval to the final version of the manuscript.

Notes

The authors declare no competing financial interest.

ACKNOWLEDGMENTS

The authors acknowledge the financial support from the Institut Carnot PolyNat (ANR-21-CARN-0025-0). The author(s) acknowledge(s) the support of the French Agence Nationale de la Recherche (ANR), under grant ANR-21-CE07-0050 (SWEET-DISPLAY). We thank the CBH-EUR-GS (ANR-17-EURE-0003) and Glyco@Alps (ANR-15-IDEX-02) for additional supports. B. C. is recognizing about the Guangzhou Elite Scholarship Council (GESC) for his scholarship

support (JY202109). We acknowledge the NanoBio ICMG (UAR 2607) for providing facilities for mass spectrometry, NMR analyses and electronic microscopy.

REFERENCES

(1) Grade, S.; Eberhard, J.; Neumeister, A.; Wagener, P.; Winkel, A.; Stiesch, M.; Barcikowski, S. Serum albumin reduces the antibacterial and cytotoxic effects of hydrogel-embedded colloidal silver nanoparticles. *RSC Adv.* **2012,** *2*, 7190–7196.

(2) Zheng, B. D.; Ye, J.; Yang, Y. C.; Huang, Y. Y.; Xiao, M. T. Self-healing polysaccharide-based injectable hydrogels with antibacterial activity for wound healing. *Carbohydr. Polym.* **2022,** *275*, 118770.

(3) Rao, K. M.; Kumar, A.; Haider, A.; Han, S. S. Polysaccharides based antibacterial polyelectrolyte hydrogels with silver nanoparticles. *Mater. Lett.* **2016,** *184*, 189–192.

(4) Li, S.; Dong, S.; Xu, W.; Tu, S.; Yan, L.; Zhao, C.; Ding, J.; Chen, X. Antibacterial Hydrogels. *Adv. Sci.* **2018,** *5* (5), 1700527.

(5) Martorana, A.; Lenzuni, M.; Contardi, M.; Palumbo, F. S.; Cataldo, S.; Pettignano, A.; Catania, V.; Schillaci, D.; Summa, M.; Athanassiou, A.; Fiorica, C.; Bertorelli, R.; Pitarresi, G. Schiff Base-Based Hydrogel Embedded with *In Situ* Generated Silver Nanoparticles Capped by a Hyaluronic Acid–Diethylenetriamine Derivative for Wound Healing Application. *ACS Appl. Mat. Interf.* **2024**, *16* (16)*,* 20186–20201.

(6) Huo, D.; Chen, B.; Meng, G.; Huang, Z.; Li, M.; Lei, Y. Ag-Nanoparticles@Bacterial Nanocellulose as a 3D Flexible and Robust Surface-Enhanced Raman Scattering Substrate. *ACS Appl. Mat. Interf.* **2020**, *12* (45)*,* 50713–50720.

(7) Lin, M.; Long, H.; Liang, M.; Chu, B.; Ren, Z.; Zhou, P.; Wu, C.; Liu, Z.; Wang; Y. Antifracture, Antibacterial, and Anti-inflammatory Hydrogels Consisting of Silver-Embedded Curdlan Nanofibrils. *ACS Appl. Mat. Interf.* **2021**, *13* (31)*,* 36747–36756.

(8) Ghasemzadeh, H.; Afraz, S.; Moradi, M.; Hassanpour, S. Antimicrobial chitosan-agarose full polysaccharide silver nanocomposite films. *Int. J. Biol. Macromol.* **2021,** *179*, 532–541.

(9) Hossein Ghasemzadeh, F. G. Antimicrobial alginate/PVA silver nanocomposite hydrogel, synthesis and characterization. *J. Polym. Res.* **2014,** *21* (355).

(10) Raveendran, P.; Fu, J.; Wallen, S. L. Completely "Green" Synthesis and Stabilization of Metal Nanoparticles. *J. Am. Chem. Soc.* **2003,** *125* (46), 13940–13941.

(11) Porter, G. C.; Schwass, D. R.; Tompkins, G. R.; Bobbala, S. K. R.; Medlicott, N. J.; Meledandri, C. J. AgNP/Alginate Nanocomposite hydrogel for antimicrobial and antibiofilm applications. *Carbohydr. Polym.* **2021,** *251*, 117017.

(12) Du, X.; Zhou, J.; Shi, J.; Xu, B. Supramolecular Hydrogelators and Hydrogels: From Soft Matter to Molecular Biomaterials. *Chem. Rev.* **2015,** *115* (24), 13165–13307.

(13) Du, X.; Zhou, J.; Xu, B. Supramolecular hydrogels made of basic biological building blocks. *Chem. Asian J.* **2014,** *9* (6), 1446–1472.

(14) Higashi, S. L.; Ikeda, M. Development of an Amino Sugar-Based Supramolecular Hydrogelator with Reduction Responsiveness. *JACS Au* **2021,** *1* (10), 1639–1646.

(15) Shen, J.-S.; Chen, Y.-L.; Huang, J.-L.; Chen, J.-D.; Zhao, C.; Zheng, Y.-Q.; Yu, T.; Yanga, Y.; Zhang, H.-W. Supramolecular hydrogels for creating gold and silver nanoparticles *in situ*. *Soft Matter* **2013,** *2013* (9), 2017–2023.

(16) Vemula, P K.; John, G. Smart amphiphiles: hydro/organogelators for *in situ* reduction of gold. *Chem. Commun.* **2006**, *21*, 2218–2220.

(17) Morris, J.; Bietsch, J.; Bashaw, K.; Wang, G. Recently Developed Carbohydrate Based Gelators and Their Applications. *Gels* **2021**, *7*, 24.

(18) Datta, S.; Bhattacharya, S. Multifarious Facets of Sugar-Derived Molecular Gels: Molecular Features, Mechanisms of Self-Assembly and Emerging Applications. *Chem. Soc. Rev.* **2015**, *44*, 5596–5637.

(19) Yao, S.; Brahmi, R.; Bouschon, A.; Chen, J.; Halila, S. Supramolecular carbohydrate-based hydrogels from oxidative hydroxylation of amphiphilic β-*C*-glycosylbarbiturates and α-glucosidase-induced hydrogelation. *Green Chem.* **2023,** *25* (1), 330–335.

(20) Yao, S.; Brahmi, R.; Portier, F.; Putaux, J. L.; Chen, J.; Halila, S. Hierarchical Self-Assembly of Amphiphilic β-*C*-Glycosylbarbiturates into Multiresponsive Alginate-Like Supramolecular Hydrogel Fibers and Vesicle Hydrogel. *Chem. Eur. J.* **2021,** *27* (67), 16716–16721.

(21) Portier, F.; Solier, J.; Halila, S. *N*,*N*′-Disubstituted Barbituric Acid: A Versatile and Modular Multifunctional Platform for Obtaining β-*C*-Glycoconjugates from Unprotected Carbohydrates in Water. *Eur. J. Org. Chem.* **2019,** *2019* (36), 6158–6162.

(22) Dekany, G.; Bornaghi, L.; Papageorgiou, J.; Taylor, S. A novel amino protecting group DTPM. *Tet. Lett.* **2001,** *42* (17), 3129–3132.

(23) Ma, M.; Kuang, Y.; Gao, Y.; Zhang, Y.; Gao, P.; Xu, B. Aromatic-aromatic interactions induce the self-assembly of pentapeptidic derivatives in water to form nanofibers and supramolecular hydrogels. *J. Am. Chem. Soc.* **2010**, *132*, 2719– 2728.

(24) Isozaki, K.; Takaya, H.; Naota, T. Ultrasound-Induced Gelation of Organic Fluids with Metalated Peptides. *Angew. Chem., Int. Ed.* **2007**, *46*, 2855–2857.

(25) Adams, D. J. Personal Perspective on Understanding Low Molecular Weight Gels. *J. Am. Chem. Soc.* **2022,** *144* (25), 11047–11053.

(26) Naota, T.; Koori, H. Molecules That Assemble by Sound: An Application to the Instant Gelation of Stable Organic Fluids. *J. Am. Chem. Soc.* **2005,** *127*, 9324–9325.

(27) Roy, B.; Bairi, P.; Nandi, A. K. Metastability in a bi-component hydrogel of thymine and 6-methyl-1,3,5-triazine-2,4-diamine: ultrasound induced *vs.* thermo gelation. *Soft Matter* **2012,** *8*, 2366–2369.

(28) Bardelang, D.; Camerel, F.; Margeson, J. C.; Leek, D. M.; Schmutz, M.; Zaman, M. B.; Yu, K.; Soldatov, D. V.; Ziessel, R.; Ratcliffe, C. I. Unusual Sculpting of Dipeptide Particles by Ultrasound Induces Gelation. *J. Am. Chem. Soc.* **2008**, 130, 3313–3315.

(29) Gómez-Sánchez, A.; Moya, P. B.; Bellanato, J. Protection of the amino group of amino sugars by the acylvinyl group: Part I, glycoside formation by the fischer reaction. *Carbohydr. Res.* **1984**,*135* (1), 101–116.

(30) Koyano, H.; Bissel, P.; Yoshihara, K.; Ariga, K.; Kunitake, T. Effect of Melamine-Amphiphile Structure on the Extent of Two-Dimensional Hydrogen-Bonded Networks Incorporating Barbituric Acid. *Chem. Eur. J.* **1997**, *3*, 1077–1082.

(31) Barnes, A. J.; Legall, L.; Lauransan, J. Vibrational spectra of barbituric acid derivatives in low-temperature matrices: Part 2. Barbituric acid and 1,3-dimethyl barbituric acid. *J. Mol. Struct.* **1979**, *56*, 15–27.

(32) Adhikari, B.; Banerjee, A. Short-Peptide-Based Hydrogel: A Template for the *In Situ* Synthesis of Fluorescent Silver Nanoclusters by Using Sunlight. *Chem. Eur. J.* **2010**, *16*, 13698–13705.

(33) Peng, H.; Yang, A.; Xiong, J. Green, microwave-assisted synthesis of silver nanoparticles using bamboo hemicelluloses and glucose in an aqueous medium, *Carbohydr. Polym.* **2013**, *91* (1), 348–355.

(34) Siddiqui, M.N.; Redhwi, H.H.; Achilias, D.S.; Kosmidou, E.; Vakalopoulou, E.; Ioannidou, M. D. Green Synthesis of Silver Nanoparticles and Study of Their Antimicrobial Properties. *J. Polym. Environ.* 2018, *26*, 423–433.

(35) Kumar, S. V.; Bafana, A. P.; Pawar, P.; Rahman, A.; Dahoumane, S. A.; Jeffryes, C. S. High conversion synthesis of <10 nm starch-stabilized silver nanoparticles using microwave technology. *Sci. Rep.* **2018**, *8* (1), 5106.

(36) Campoccia, D.; Montanaro, L.; Arciola, C. R. A review of the biomaterials technologies for infection-resistant surfaces. *Biomaterials* **2013**, *34* (34), 8533–8554.

(37) Eckhardt, S.; Brunetto, P. S.; Gagnon, J.; Priebe, M.; Giese, B.; Fromm, K. M. Nanobio silver: its interactions with peptides and bacteria, and its uses in medicine. *Chem. Rev.* **2013**, *113* (7), 4708–4754.

(38) Van Hamme, J. D.; Singh, A.; Ward, O. P. Physiological aspects: Part 1 in a series of papers devoted to surfactants in microbiology and biotechnology. *Biotechnol. Adv.* **2006**, *24*, 604–620.

(39) Dane, E. L.; Ballok, A. E.; O'Toole, G. A.; Grinstaff, M. W. Synthesis of bioinspired carbohydrate amphiphiles that promote and inhibit biofilms. *Chem. Sci.* **2014**, *5*, 551–557.

(40) Martínez-Castañón, G.A.; Niño-Martínez, N.; Martínez-Gutierrez, F.; Martínez-Mendoza, J.R.; Ruiz F. Synthesis and antibacterial activity of silver nanoparticles with different sizes. *J. Nanopart. Res.* **2008**, *10*, 1343–1348.

For Table of Contents Only